# A High-Performance Nitro-Explosives Schottky Sensor Boosted by Interface Modulation

*Zheng Yang, Xincun Dou,* Shengli Zhang, Linjuan Guo, Baiyi Zu, Zhaofeng Wu, and Haibo Zeng**

**A high-performance Schottky sensor boosted by interface modulation is fabricated for the detection of trace nitro-explosives vapors. The interface modulation strategy results in a silicon nanowires (SiNWs) array/$TiO_2$/reduced graphene oxide (rGO) sensor with sensitive and selective response toward nitro-explosives vapors. The response of the SiNWs array/$TiO_2$/rGO sensor toward nitro-explosives vapors, such as 9 ppb 2,4,6-trinitrotoluene, 4.9 ppt hexogen, and 0.25 ppq octagon, is boosted by 2.4, 7.5, and 5 times with the insertion of $TiO_2$. Superior selectivity is shown even compared with interfering gases of 10 ppm. Such good sensing performance can be attributed to the good sensing performance of the Schottky heterojunction-based sensor, the Schottky barrier height modulation with the insertion of $TiO_2$, SiNWs array structure enhanced diffusion, and $TiO_2$ nanoparticles enhanced adsorption. This is believed to be the first Schottky heterojunction-based sensor for nitro-explosives vapors detection. This work would open a new way to develop highly sensitive and selective sensors.**

## 1. Introduction

Nanosensors are powerful potential sensors for the detection of trace chemical species including nitro-explosives due to the large surface-to-volume ratios and high reaction activities.[1–7] However, most of the sensors are in the form of chemiresistor or Chem-field-effect transistor (Chem-FET), in which the conductance of the device is changed by the surface-adsorbed molecules and depends highly on the analyte concentrations.[8–12] As a result, the traditional Ohm-contacted nanosensor has difficulty in realizing the ultrasensitive detection in real circumstances where open environment must be considered. Recently, it was demonstrated that Schottky contact could largely improve the sensitivity of nanosensors due to that Schottky barrier serves as a "gate" controlling the current passing through the barrier,[13,14] and the value of this current highly depends on the Schottky barrier height (SBH). A small change in SBH will lead to a huge change in current, which is the basis of the Schottky barrier enhanced sensing.[13] The selection of the components of the Schottky junction is of vital importance to improve the sensor performance, which highly depends on the energy band structure and adsorption characteristics. It is reported that a higher SBH favors a better sensitivity in a Schottky-gated sensor toward electron acceptor analytes detection, while for electron donor analytes detection, the result is opposite.[15] Thus, the insertion of another semiconductor that could both modulate the SBH and increase the adsorption energy will greatly increase the sensitivity and selectivity in a Schottky junction sensor. Graphene or reduced graphene oxide (rGO) with high charge carrier mobility, atomically thin nature and abundant adsorption sites,[16–20] makes the semiconductor/graphene Schottky heterojunction (Barristor) ultrasensitive for gas sensing.[21,22] Vertical silicon nanowires (SiNWs) array offers distinct merits in terms of the capability for surface functionalization and the sufficient gaps for molecules diffusion, and SiNWs array-based sensor has been considered an ideal platform for gas sensing due to the higher signal-to-noise ratios and faster response.[23,24] The electron affinity of $TiO_2$ (4.0 eV) is only a bit smaller than that of silicon (4.05 eV);[25] thus the insertion of $TiO_2$ into Si/rGO should be an ideal choice to support the above assertion. As a result, the SiNWs array/$TiO_2$/rGO ternary junction will provide a new approach for designing ultrasensitive and selective sensors.

Nitro-explosives is one of the most important categories in common explosives, and the detection of them has been a research focus due to plenty of adverse events, increasing threat of terrorism attack, and the need for homeland security.[1,9,26,27] The sensitive, selective, and rapid detection of nitro-explosives vapors is still a challenge due to the low vapor pressure of

Z. Yang, Prof. X. C. Dou, L. J. Guo, Dr. B. Y. Zu, Dr. Z. F. Wu
Laboratory of Environmental Science and Technology
Xinjiang Technical Institute of Physics and Chemistry
Key Laboratory of Functional Materials and Devices for Special Environments
Chinese Academy of Sciences
Urumqi 830011, China
E-mail: xcdou@ms.xjb.ac.cn
Z. Yang, L. J. Guo
University of Chinese Academy of Sciences
Beijing 100049, China
Dr. S. L. Zhang, Prof. H. B. Zeng
Institute of Optoelectronics and Nanomaterials
College of Materials Science and Engineering
Nanjing University of Science and Technology
Nanjing 210094, China
E-mail: zeng.haibo@njust.edu.cn

**DOI: 10.1002/adfm.201501120**

nitro-explosives, such as the room temperature-saturated vapor pressures of 2,4,6-trinitrotoluene (TNT), dinitrotoluene (DNT), para–nitro toluene (PNT), picric acid (PA), hexogen (RDX), and octagon (HMX) are 9 ppb (part per billion), 411 ppb, 647 ppb, 0.97 ppb, 4.9 ppt (part per trillion), and 0.25 ppq (part per quadrillion), respectively.[28] These nitro-explosives vapors will be ideal analytes to illustrate the above Schottky junction design.

In this paper, we put forward and demonstrate the interface modulation strategy to greatly improve the sensing performance of a Schottky sensor. The responses of the SiNWs array/$TiO_2$/rGO sensor toward nitro-explosives vapors, such as 9 ppb TNT, 4.9 ppt RDX, and 0.25 ppq HMX, were boosted by 2.4, 7.5, and 5 times with the insertion of $TiO_2$. Superior selectivity was shown even compared with interfering gases of 10 ppm. To the best of our knowledge, this is the first Schottky heterojunction-based sensor for nitro-explosives vapors detection. This work would open a new way to develop highly sensitive and selective sensors.

## 2. Results

### 2.1. Construction of the SiNWs Array/$TiO_2$/rGO Schottky Heterojunction-Based Sensor

The fabrication process of the SiNWs array/$TiO_2$/rGO Schottky heterojunction-based sensor is illustrated in **Figure 1**. The detailed information can be seen in the Experimental Section. Briefly, SiNWs (n-type, $\rho$ = 1–10 Ω cm) array was synthesized via the wet-etching method[29,30] (Figure 1a). Then, the n-type $TiO_2$ layer was decorated according to our previous reports[31,32] (Figure 1b). GO layers were spin coated onto the top of the vertically aligned $TiO_2$ nanoparticles decorated SiNWs, and subsequently reduced by hydrazine vapor, dried by $N_2$ blowing, and annealed in $N_2$ to form the SiNWs array/$TiO_2$/rGO Schottky heterojunction (Figure 1c). Finally, the Schottky heterojunction was fabricated into a home-made sensing device (Figure 1d).

Cross-sectional and planar field-emission scanning electron microscopy (FESEM) views show that the as-etched SiNWs are vertically aligned, highly ordered and about 12 μm in length (**Figure 2**a). The top of the SiNWs array is fully covered with $TiO_2$ nanoparticles and the side surface is successfully decorated (Figure 2b). Transmission electron microscope (TEM) observation shows that the edge and the top of the SiNWs are successfully decorated with $TiO_2$ nanoparticles (Figure 2c). High-resolution transmission electron microscope (HRTEM) characterizations further show that the decorated $TiO_2$ nanoparticles with an ellipsoid shape are anatase in phase and have an average size of about 10 nm (Figure 2d and Figure S1, Supporting Information). Planar FESEM view of the SiNWs array/$TiO_2$/rGO heterojunction shows that the rGO top electrode lies tightly on the top of the array (Figure 2e). The RGO top electrode has only several layers and it attaches with the tip of the $TiO_2$ nanoparticles decorated SiNWs array firmly, making a good contact (inset in Figure 2e). Raman spectrum of the SiNWs array/$TiO_2$/rGO heterojunction shows two strong characteristic bands at 1342 and 1542 $cm^{-1}$ (Figure 2f). The intensity ratio of the two bands ($I_D/I_G$) is ≈1.1, indicating the existence of extensive defects that can be the active sites for gas adsorption.[20]

### 2.2. Basic Working Principles of the SiNWs Array/$TiO_2$/rGO Schottky Heterojunction-Based Sensor

The sensing characteristics of the resulting sensor were then evaluated by *I–V* curves and band structure analysis. Typical *I–V* curves of the sensor exhibit nonlinear behaviors, with forward/reverse current ratios of ≈3 at ±4 V (**Figure 3**a), implying the successful formation of the Schottky barrier.[15,25,33] This result is consistent with the recently reported results that Schottky gate could be constructed by the contact between n-type silicon and graphene.[22,34] The *I–V* characteristic of the Si/rGO device can be expressed by the thermionic emission model[35]

$$I = I_s\left[\exp\left(\frac{qV}{\eta kT}\right)-1\right] = AA^*T^2\exp\left(-\frac{\Phi_B}{KT}\right)\left[\exp\left(\frac{qV}{\eta kT}\right)-1\right] \quad (1)$$

where $I_s$ is the reverse saturation current, $q$ is the electronic charge, $A$ is the contact area, $A^*$ is the effective Richardson constant, $\eta$ is the diode ideality factor, $T$ is the absolute temperature, $\Phi_B$ is the SBH, and $k$ is the Boltzmann constant. SBH can be determined with the knowledge of the $\eta$, $I_s$, which can be derived from the *I–V* curves and $T$, $A$ and Richardson's constant $A^*$, which are known parameters. Using the *I–V* curves and the

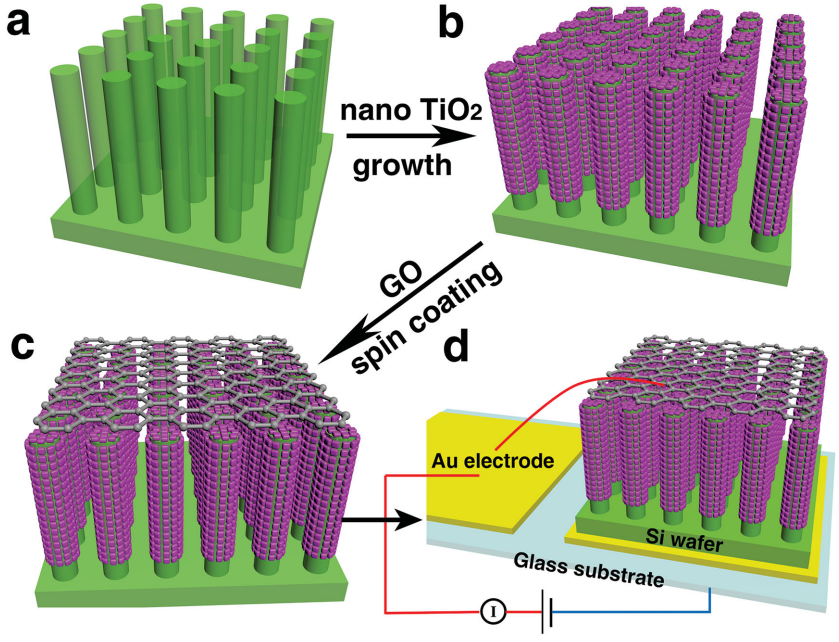


**Figure 1.** Schematic illustration of the Schottky heterojunction fabrication-based nanosensor process. a) SiNWs array. b) $TiO_2$ nanoparticles decorated SiNWs array. c) SiNWs array/$TiO_2$/rGO Schottky heterojunction and d) the constructed nanosensor.

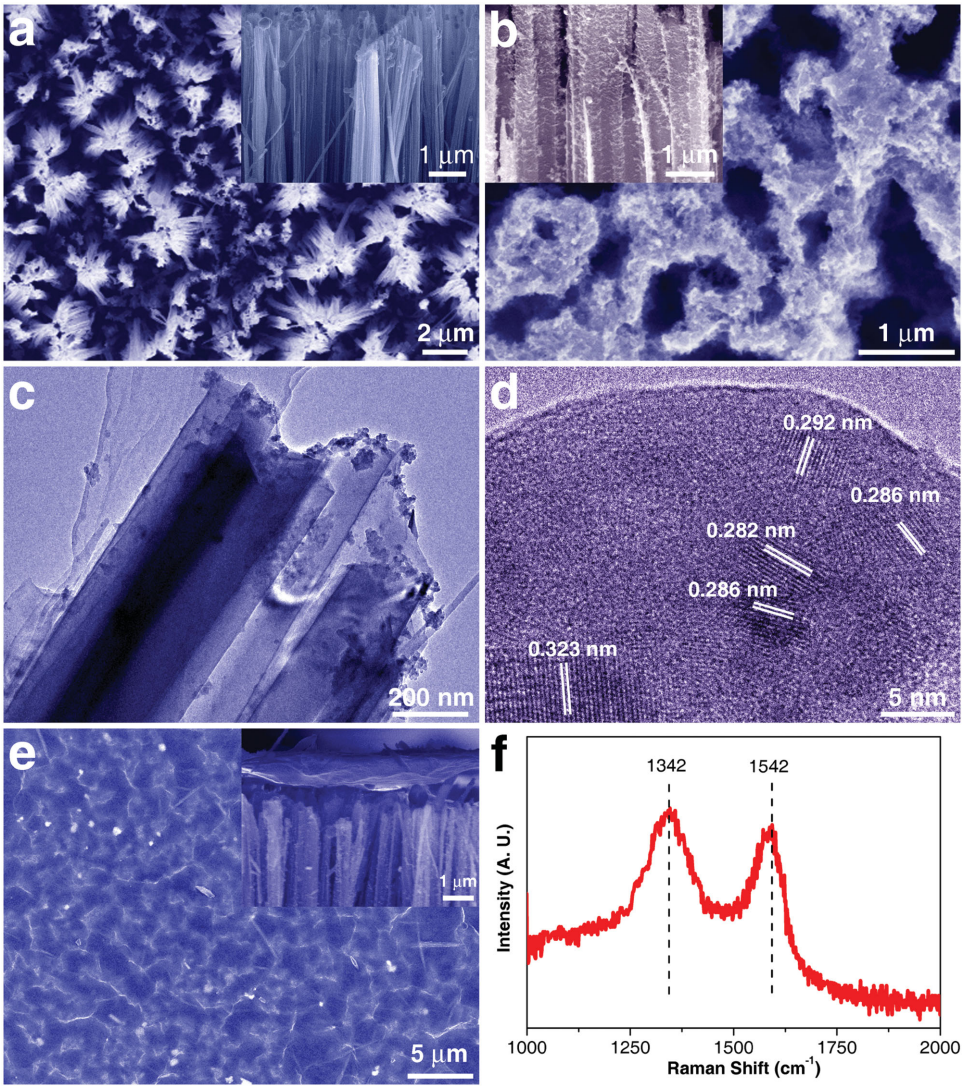


**Figure 2.** a) Planar view of the SiNWs array (inset: cross-sectional view). b) Planar view of the $TiO_2$ nanoparticles decorated SiNWs array (inset: cross-sectional view). c) TEM image of the $TiO_2$ nanoparticles decorated SiNWs. d) HRTEM image of the tip of a $TiO_2$ nanoparticles decorated SiNW. e) Planar view of the SiNWs array/$TiO_2$/rGO Schottky heterojunction (inset: cross-sectional view). f) Raman spectrum of the SiNWs array/$TiO_2$/rGO Schottky heterojunction.

measured area of 0.0225 $cm^2$ and $A^*$ values of 1200 A $cm^{-2}$ $K^{-2}$ for $TiO_2$,[36] we find $\eta = 0.6$, $I_s = 1.1$ nA, and $\Phi_B = 0.919$ eV for the air atmosphere, and $\eta = 0.6$, $I_s = 4.4$ nA, $\Phi_B = 0.883$ eV for the TNT atmosphere.

From this equation, it can be clearly seen that the reverse current (both saturation current and unsaturation current) highly depends on SBH (exponential relationship). The current across the sensor decreases from –1.7 to –1.82 μA at a reverse bias of –4.0 V when air was replaced by TNT-saturated vapor, and it further decreases to –2.3 μA when exposed to DNT-saturated vapor. However, the current of the sensor changes only a bit when it was put into TNT- and DNT-saturated vapors (5.35 and 5.57 μA) from air (5.25 μA) at a forward bias of 4.0 V, indicating a higher response of the sensor under reverse bias. Compared with the energy band structure of the Si/rGO heterojunction with no bias (Figure S2, Supporting Information), the SBH of the SiNWs array/$TiO_2$/rGO Schottky heterojunction (Figure 3b) is higher. The insertion of $TiO_2$ into the Si/rGO Schottky heterojunction helps to change the band structure, and thus reconfigure the SBH and enhance the sensitivity toward electron-withdrawing molecules such as TNT.

In the forward bias mode (here, reverse and forward biases are defined as negative or positive voltage applied to the rGO layers, respectively), the current is mainly contributed by the thermionic emission and diffusion, and SBH has little effect on them (Figure 3c).[37] The nitro-explosives molecules have to adsorb on the surface of Si and change the surface conductance, resulting in a small response, which is similar to the traditional chemiresistor. On the contrary, as can be seen in Figure 3d, at an applied reverse bias, the electrons have to overcome the energy barrier to transport through the rGO top electrode. The adsorption of TNT molecules would decrease the SBH; thus, combined with the formula above, the number of electrons that flow across the Schottky heterojunction interface

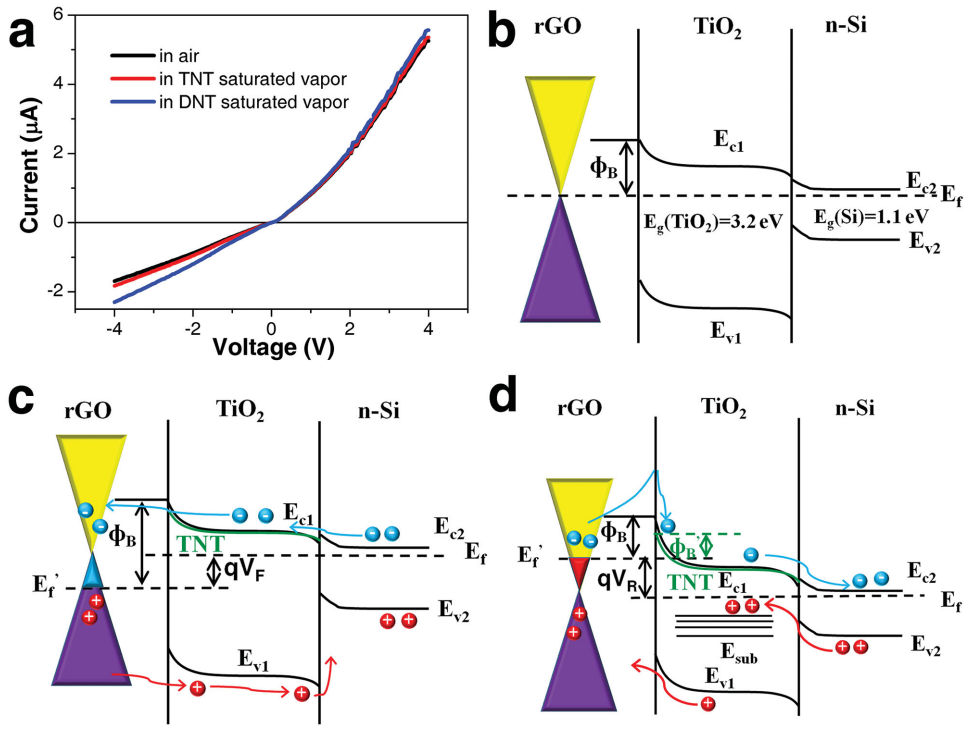


**Figure 3.** a) *I–V* curves of the SiNWs array/$TiO_2$/rGO Schottky heterojunction-based nanosensor taken in air, in room temperature-saturated vapors of TNT and DNT (9 and 411 ppb). b) Thermal equilibrium energy band diagram of Si/$TiO_2$/rGO heterojunction. Energy band diagrams of the heterojunction showing the carriers transfer process under c) forward bias, and d) reverse bias. $V_F$ is the forward bias, $V_R$ is the reverse bias, $E_f'$ is the quasi Fermi level of rGO, and $\Phi_B$ is the Schottky barrier height. The blue surface on the Dirac cone of graphene in (c) denotes the electrons injected from $TiO_2$, while the red one in (d) denotes the holes injected from $TiO_2$.

would be increased significantly and a great increase of the current is expected. In other words, the current is dominated by SBH and the Schottky barrier plays an important role. This effect is much more pronounced for the reverse bias mode than for the forward bias mode since the electrons need to overcome the Schottky barrier to form current from the rGO to the semiconductor domain ($TiO_2$) under the reverse bias mode.[13]

### 2.3. Sensing Properties toward Nitro-Explosives Vapors

The gas-sensing characteristics of the sensor under reverse and forward biases toward TNT-saturated vapor were then investigated and compared with each other. For reverse bias sensing, a constant current of –1 μA was applied during the measurement. Here, the constant current measurement mode is beneficial to minimize the background noises. For comparison, a constant current of 1 μA was applied for the forward bias sensing. (From the *I–V* curve, we can find that the reverse current of –1 μA corresponds to the bias of –2.3 V while 1 μA correspond to 1.15 V.) It is reported that with the substantial increase of the reverse bias, the response values increase slowly,[15] while no evidence shows that the response in Ohm-contacted nanosensor or under forward bias is influenced by the bias value. As a result, the selected constant current has little impact on the sensitivity of the sensor. The resistance change of the sensor under reverse bias is almost the same and can recover to the initial value during three successive cycles (**Figure 4**a), indicating the good repeatability of the sensor. Compared with the forward bias sensing (Figure 4b), which shows a much lower signal-to-noise ratio, the advantage of reverse bias sensing is obvious.

The sensor response toward room temperature-saturated vapor of TNT under forward bias is less than 1%, while that under reverse bias is more than 6%, indicating the superior advantage under reverse bias sensing. The reverse bias sensing properties of the sensor toward saturated vapors of DNT, PA, RDX, HMX, and PNT were further evaluated (Figure S3, Supporting Information). Molecular formulas and saturated vapor pressures are shown in Figure S4 and Table S1 (Supporting Information). It is noticed that the responses of the sensor toward different nitro-explosives under reverse bias are all much higher than those under forward bias (Figure 4c). Furthermore, the responses toward nitro-explosives are much higher than those toward $NO_2$ and $NH_3$ (typical electron accepter and donor species) since the vapor pressures of nitro-explosives are much lower than the gas concentrations of $NO_2$ and $NH_3$ (10 ppm). Our preliminary tests have partly shown the real-world sensing capability to detect the nitro-explosives vapors, namely the anti-interference performance toward common interfering gases, $NO_2$ and $NH_3$.

As shown in Figure S5 (Supporting Information), the responses of the sensor toward four different concentrations of TNT, DNT, PNT, PA, RDX, and HMX are recorded and fitted as a function of concentrations, respectively. The estimated limits of detection (defined as LOD = $3S_D/m$, where $m$ is the slope of

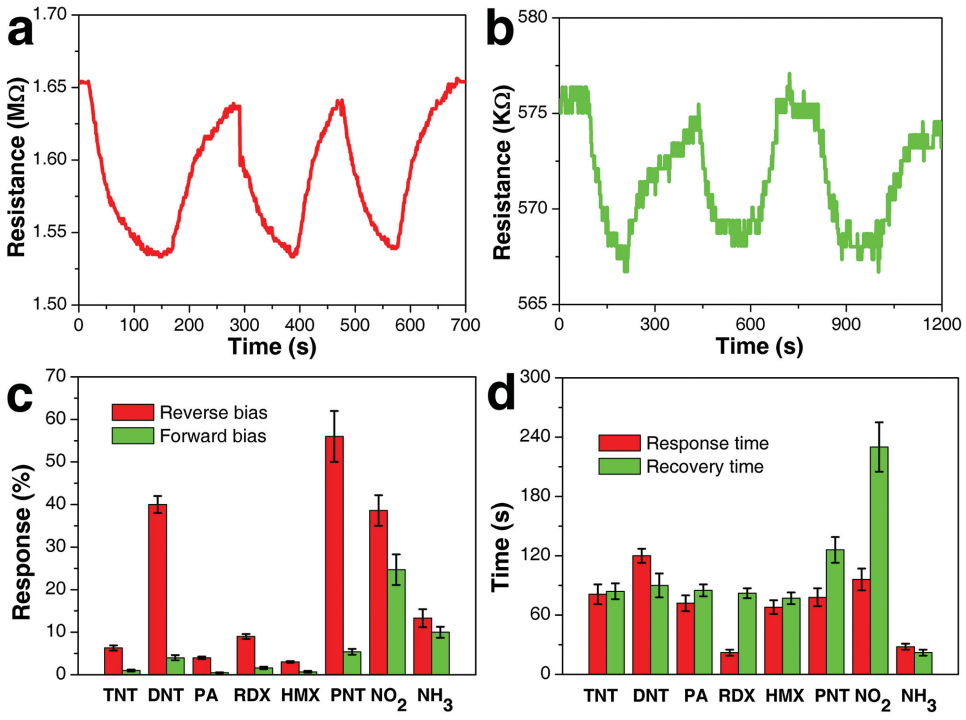


**Figure 4.** Resistance change of the SiNWs array/$TiO_2$/rGO Schottky heterojunction-based sensor under a constant a) reverse current of –1 μA and b) forward current of 1 μA during three successive cycles of exposure toward room temperature-saturated vapor of TNT. c) Comparison of the responses of the sensor under reverse and forward biases toward room temperature-saturated vapors of TNT, DNT, PA, RDX, HMX, and PNT, $NO_2$ (10 ppm) and $NH_3$ (10 ppm). d) The corresponding response time and recovery time of the sensor under reverse bias.

the linear part of the calibration curve and $S_D$ is the standard deviation of noise in the response curve) for TNT, DNT, PNT, PA, RDX, and HMX are determined to be 0.77 ppb, 6.5 ppb, 74 ppb, 0.12 ppb, 0.5 ppt, and 0.05 ppq, respectively. Sensor stability and reproducibility are another two key criterions for practical applications. The reproducibility can be seen in Figure 4a and S3 (Supporting Information), in which response of each cycle always keeps the same value. To verify the stability, over 20 sensors were fabricated and tested, and it is found that the responses of the sensors are stable and the deviations between different sensors are less than 20%. Furthermore, the response curves toward saturated TNT vapor after 3 months and after 9 months are compared with that of the fresh device (Figure S6, Supporting Information). It is observed that the sensor response decreases from 6.3% to 5.7% after 9 months, showing the good stability.

All the response time and recovery time of the sensor toward the above eight vapors are less than 120 s except for the recovery time of $NO_2$ (Figure 4d). Compared with the sensor working under forward bias (Figure S7, Supporting Information), the response time and recovery time are effectively reduced. For example, the response time and recovery time toward TNT under reverse bias are 81 and 84 s respectively, while those under forward bias are 123 and 165 s.

The comparison of our SiNWs array/$TiO_2$/rGO Schottky heterojunction-based sensor and other explosives vapors sensors and graphene-based Schottky gas sensors is listed in **Table 1**. Compared with other traditional Ohm-contacted explosives vapors sensors, the present SiNWs array/$TiO_2$/rGO Schottky heterojunction-based sensor shows a higher sensitivity toward TNT[1,12] and DNT[10,12] due to the Schottky junction and

**Table 1.** Comparison of different gas-phase nitro-explosives sensors and Si/graphene-based sensors.

| Sensing material | Analytes and concentration | Responses | Ref. |
|---|---|---|---|
| ZnO nanowire | TNT, 60 ppb | 20% | [1] |
| SWNT | TNT, 8 ppb | 5% | |
| Titania(B) nanowires | TNT, 9 ppb | 47% | [10] |
| | DNT, 180 ppb | 38% | |
| GaN nanowire-titania nanocluster hybrids | TNT, 9 ppb | 5% | [12] |
| | DNT, 411 ppb | 20% | |
| | PNT, 647 ppb | 20% | |
| Covalently functionalized | Nitromethane, 57 ppm | 0.1% | [3] |
| SWNT | Cyclohexanone, 57 ppm | 0.5% | |
| Organic nanoribbons | 4-PNT 100 ppm | 15% | [38] |
| | DNT 100 ppb | 40% | |
| | Nitromethane 36 000 ppm | 65% | |
| DNA decorated SWNT | 1.57 ppm DMMP | 7.5% | [39] |
| Si/graphene Schottky heterojunction, reverse bias | $NO_2$, 200 ppb, 20 ppm | 9%, 400% | [15] |
| | $NH_3$, 10 ppm | 30% | |
| Graphene/SiNWs heterojunction, forward bias | $O_2$, 2500 sccm in air | 40% | [33] |
| | $H_2$, 2500 sccm in air | 1000% | |

interface modulation. What is more, compared with those sensors toward gases with rather high concentrations,[3,38,39] our sensor can detect HMX vapor at sub-ppq level. Compared with other Si/graphene-based sensors that are sensitive to common gases,[15,33] our sensor shows excellent selectivity, making it more suitable for real application.

### 2.4. Advantages of Structure and Sensing Performance

Different from the reported Si/graphene Schottky heterojunction-based sensors,[15,21] in this report, we used the SiNWs array instead of the silicon wafer to improve the sensitivity. In order to prove it, a SiNWs array/rGO and a Si/rGO Schottky heterojunction-based sensors were fabricated (insets in **Figure 5**a,b). Typical *I*–*V* curves of them taken in air, in room temperature-saturated vapors of TNT and DNT exhibit a nonlinear behavior (Figure 3a,b). Using the *I*–*V* curves and the measured area of 0.036 $cm^2$ and $A^*$ values of 252 A $cm^{-2}$ $K^{-2}$ for n-Si,[25] we find $\eta$ = 5.72, $I_s$ = 7.2 nA, $\Phi_B$ = 0.84 eV for the SiNWs array/rGO in the air, and this SBH is smaller than that of SiNWs array/$TiO_2$/rGO Schottky heterojunction. The current of the SiNWs array/rGO-based sensor is much smaller than that of the Si/rGO-based sensor at the same bias due to the fact that though the device sizes for the Si/rGO-based sensor (≈4 $mm^2$) and the Si/rGO-based sensor (≈2.25 $mm^2$) are comparable, the contact area for the SiNWs array is much smaller, which can be seen in Figure 2a (the occupied area percentage of SiNWs is less than 20%). Thus, the amount of the charge carriers passing through the SiNWs array is much less. The current across the SiNWs array/rGO-based sensor decreases from –5.7 to –5.85 μA at a reverse bias of –4.0 V when air was replaced by TNT-saturated vapor, and it further decreases to –7.5 μA when exposed to DNT-saturated vapor (Figure 5a). However, the *I*–*V* curves of the Si/rGO-based sensor in air, TNT, and DNT-saturated vapor almost overlap at the same bias (Figure 5b), indicating that the SiNWs array is more beneficial for the detection of TNT and DNT than Si wafer.

The SiNWs array/rGO-based sensor shows a response of 30.5% toward saturated DNT vapor under a constant applied current of –1 μA (Figure 5c), while the Si/rGO-based sensor only shows a response of 4.1%. Similarly, the responses of both sensors toward room temperature-saturated vapors of TNT, DNT, PA, RDX, HMX, PNT and diluted $NH_3$ and $NO_2$ gases were investigated (Figure 5d). With the introduction of the SiNWs array structure, the sensing responses to all the target gases were significantly improved, especially to DNT and $NH_3$. It is found that all the response times of the SiNWs array/rGO-based sensor are less than 60 s (Figure 5e). Undoubtedly, the SiNWs array structure decreases the response time due to the efficient utilization of the entire top area of an individual nanowire and both surfaces of the rGO sheets. However, the recovery time of the SiNWs array/rGO-based sensor is relatively longer (Figure 5f), which could be attributed to the abundant adsorption sites induced desorption difficulties.

The SiNWs array has some advantages over silicon wafer. Nitro-explosives molecules, such as TNT, can only adsorb on the top of the rGO sheets and change the current crossing the Schottky heterojunction interface (**Figure 6**a). However, TNT molecules are more likely to diffuse into the gaps between SiNWs and adsorb on both sides of the rGO sheets and the nanowire surface to change the SBH (Figure 6b). Taking TNT as an example, when the vapor concentrations are the same for both devices, much more TNT molecules can adsorb on the SiNWs array/$TiO_2$/rGO heterojunction interface and the change in SBH is bigger.

To further illustrate the advantages of the SiNWs array/$TiO_2$/rGO Schottky heterojunction-based sensor toward nitro-explosives vapors, the sensing properties of it with the SiNWs array/rGO sensor were compared. It is found that although the response time of the SiNWs array/$TiO_2$/rGO-based sensor increased a bit (Figure S8, Supporting Information), the recovery time was greatly cut down, which is of vital importance in practical application. From the response comparison (Table S2, Supporting Information), one can see that with the introduction of $TiO_2$, the responses of the SiNWs array/rGO Schottky heterojunction-based sensor increase remarkably; typically, from 2.6%, 1.2% and 0.6% to 6.3%, 9.0% and 3.0% for TNT, RDX, and HMX, respectively. The SiNWs array/$TiO_2$/rGO Schottky heterojunction-based sensor shows a much lower response (13.3%) toward electron donor ($NH_3$) compared with the SiNWs array/rGO Schottky heterojunction-based sensor (45.8%), while the responses toward the rest electron accepter molecules are higher, confirming the above assertion. Thus, the sensitivity toward reducing gases can be easily weakened. Although the response toward $NO_2$ increases 1.3 times, the responses for nitro-explosives increase larger, especially 2.4 times for TNT, 7.5 times for RDX, and 5 times for HMX (**Figure 7**). The above results clearly show that the SiNWs array/$TiO_2$/rGO-based sensor is much more beneficial for the sensitive and selective detection toward nitro-explosives due to the introduction of $TiO_2$ nanoparticles.

### 2.5. Theoretical Analysis of the Adsorption Energy

The further theoretical analysis supports the above experimental data. The adsorption energy of a SiNW and the $TiO_2$ nanoparticles decorated SiNW toward TNT, DNT, or PNT molecules was calculated (**Figure 8**). It is clearly shown that the adsorption energy toward TNT and DNT increases with the decoration of $TiO_2$ nanoparticles, indicating an improved and selective detection is preferred with the above SiNWs array/$TiO_2$/rGO Schottky heterojunction. And it is considered that the adsorptivity toward PNT almost does not change after the decoration of $TiO_2$ nanoparticles since an equivalent adsorption energy is observed. As a result, the improvement in the response of the SiNWs array/$TiO_2$/rGO Schottky heterojunction-based sensor toward PNT can be attributed to the increase of SBH induced by the decoration of $TiO_2$ nanoparticles at the interface of SiNWs array and rGO top electrode.

## 3. Discussions

Based on the above analysis, the good sensing performance of the SiNWs array/$TiO_2$/rGO Schottky heterojunction-based sensor toward nitro-explosives vapors could be attributed to

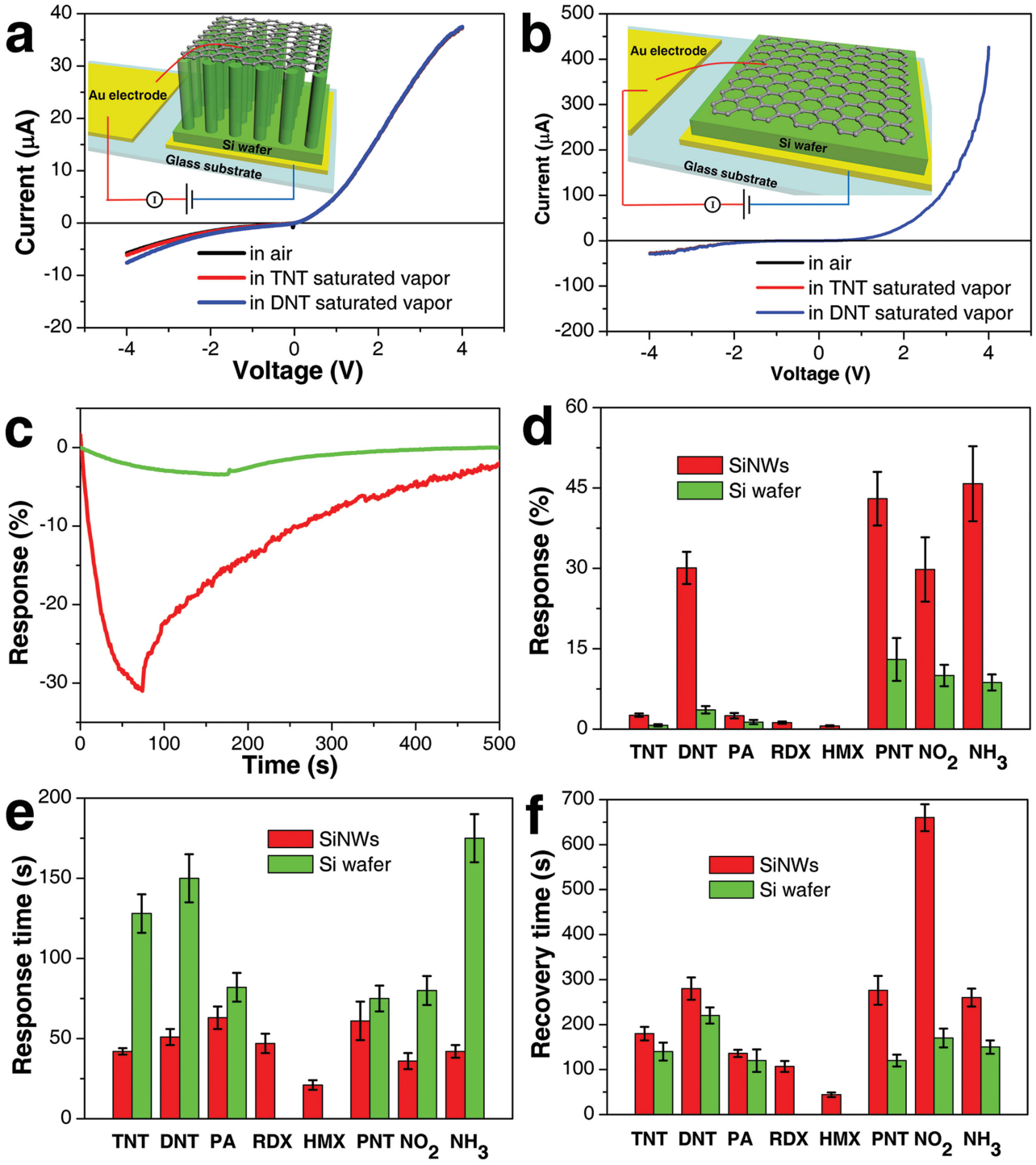


**Figure 5.** *I–V* curves of a) SiNWs array/rGO and b) Si/rGO Schottky heterojunction-based sensors taken in air, in room temperature-saturated vapor of TNT and DNT (9 and 411 ppb). c) Comparison of the response curves of the two sensors toward DNT vapor under reverse bias (–1 μA). Comparison of d) response, e) response time, and f) recovery time of the two sensors toward room temperature-saturated vapors of TNT, DNT, PA, RDX, HMX, and PNT, $NO_2$ (10 ppm) and $NH_3$ (10 ppm).

the following three reasons: (1) Schottky barrier modulation with the insertion of $TiO_2$; (2) SiNWs array structure enhanced diffusion; and (3) $TiO_2$ nanoparticles enhanced adsorption. As a result, highly sensitive and selective sensors toward nitro-explosives vapors detection could be realized by the introduction of the Schottky gated sensing method, and further improved by rational design of the sensor components and structures.

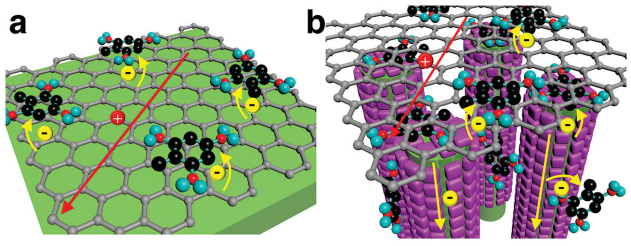


**Figure 6.** Schematic sensing mechanisms of a) Si/rGO and b) SiNWs array/$TiO_2$/rGO Schottky heterojunction-based sensors.

In the future work, the sensitivity of the present system should be further improved by using monolayer rGO sheet to form the top electrode, optimizing the SBH and minimizing the device size. The Fermi level of graphene needs to be intentionally adjusted to enhance the sensitivity. The specific metal oxide of which the adsorption energy toward explosive molecules is much higher than other interfering gases should be chosen for interface modulation. Furthermore, to achieve the goal of instant detection, the response time should be further decreased by decorating specific groups and the desorption process should be enhanced by introducing light illumination.

## 4. Conclusions

In summary, the interface modulation strategy was adopted to greatly improve the sensing performance of a Schottky sensor. A reverse-biased SiNWs array/$TiO_2$/rGO Schottky heterojunction-based sensor with high sensitivity and good selectivity toward nitro-explosives vapors has been demonstrated. With the introduction of $TiO_2$, the responses toward trace nitro-explosives vapors increase remarkably, especially toward ppb-level TNT, ppt-level RDX, and sub-ppq-level HMX. Excellent selectivity was shown even compared with reducing or oxidizing interfering gases of 10 ppm. The nice performance of the sensor is first attributed to the decoration of $TiO_2$, which not only increases the SBH, but also increases the adsorption energy toward nitro-explosives. The concept illustrated here presents a new sensing method that can be applied to the ultrasensitive detection of trace molecules such as nitro-explosives vapors.

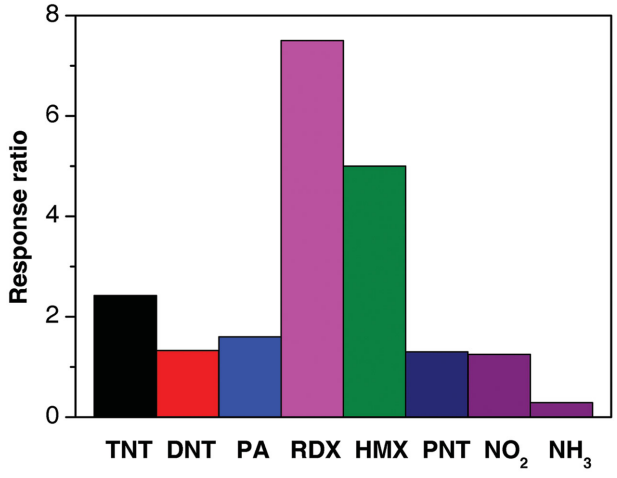


**Figure 7.** Response ratios of the SiNWs array/$TiO_2$/rGO-based sensor over the SiNWs array/rGO-based sensor.

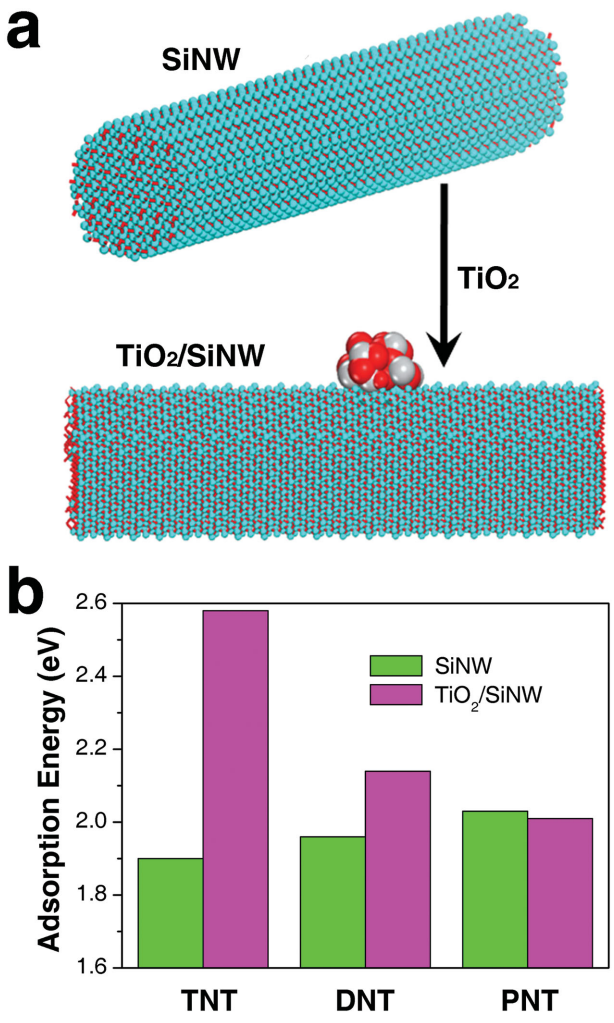


**Figure 8.** Calculation of the adsorption energy of SiNWs and $TiO_2$ nanoparticles decorated SiNWs toward nitro-explosives molecules. a) Model and b) adsorption energy of TNT, DNT, and PNT.

## 5. Experimental Section

*Chemicals*: 2,4-Dinitrotoluene, PNT, and PA were purchased from Sigma-Aldrich. TNT, RDX, and HMX were obtained from the National Security Department of China. TNT was recrystallized with ethanol before use. Graphite powder (SP-1 grade, 325 mesh) was purchased from Bay Carbon, Inc. All other chemicals were of analytical grade and used without further purification.

*Caution*: TNT and other nitro-explosives used in the present study are highly explosive and should be handled only in small quantities.[5,40]

*Preparation of SiNWs Array*: SiNWs array was synthesized following the reported results.[29,30] Briefly, Si(100) wafers (n-type, $\rho$ = 1–10 Ω cm, moderately doped, $N_D < 10^{17}$ $cm^{-3}$) were cut into rectangular strips and sequentially cleaned with acetone, ethanol, a piranha solution (98% $H_2SO_4$/30% $H_2O_2$, v/v = 4/1), deionized water, and diluted HF solution. The cleaned silicon strips were then immediately immersed into the

etching solution (containing 4.6 M HF and 0.02 M $AgNO_3$) in a Teflon autoclave and treated at 50 °C for 1 h. After the etching process, the obtained samples were rinsed in nitride acid to remove silver, washed with deionized water, and dried by $N_2$ blowing. Oxygen plasma treatment was conducted finally.

*Decoration of $TiO_2$ Nanoparticles*: $TiO_2$ nanoparticles were decorated according to our previous reports.[31,32] Briefly, 0.55 mL of $TiCl_4$ kept in a refrigerator was extracted using a 1 mL syringe and rapidly injected into the bottom of a parafilm sealed 100 mL bottle with 50 mL of DI water in the form of ice. After that, the bottle was firmly covered with the bottle cap and shaken continuously until the ice was dissolved. In the whole process, no white precipitation was observed. Then, the SiNWs array was immersed into the $TiCl_4$ solution and kept in an oven at 70 °C for 6 h. The resulting samples were then rinsed with deionized water, dried at 70 °C for 3 h, and annealed in a tubular oven at 500 °C for 1 h in air.

*RGO Top Electrode Construction*: GO was synthesized using a modified Hummers method,[41,42] and diluted into a solution with a concentration of 1 mg $mL^{-1}$. GO solution was spin-coated on the SiNWs array (wetted for 1 min, spun at 600, 800, and 1600 rpm in sequence and each process for 1 min), dried in vacuum at 80 °C for 3 h, and reduced by hydrazine vapor at 40 °C for 18 h. Finally, the sample was rinsed with deionized water, dried by $N_2$ blowing, and heat treated at 400 °C for 3 h in $N_2$.[43]

*Characterization*: Field-emission scanning electron microscope (FESEM, ZEISS SUPRA 55VP) and transmission electron microscope (JEM-2011 TEM, 200 kV) were used to characterize the morphology of the samples.

*Device Fabrication, Electrical Properties, and Gas-Sensing Properties Testing*: The sizes of the sensors are all about 1.5–2 mm × 1.5–2 mm. The top contact was produced by depositing an Au square with a 1 mm breadth diameter using a mask on the top of the heterojunction. After that silver paste was used to connect the Au square and copper wire. The *I–V* curves and gas sensing properties were recorded by electrochemical workstation (CIMPS-2, ZAHNER). The room temperature-saturated explosive vapor was obtained by putting solid explosive powder (1 g) at the bottom of a conical flask (50 mL) before it was sealed for 48 h. For the gas-sensing test, the sensor was inserted into the saturated vapor of an explosive. After the sensor voltage reached a new constant value, the sensor was then inserted into a same conical flask full of air to recover.

*Definition of Sensor Response, Response Time, and Recovery Time*: The relative sensor response in resistance is defined as, Response = $(R_g - R_a)/R_a \times 100\%$, where $R_g$ and $R_a$ are the electrical resistances of the sensor in explosive vapor and in air. The response time was defined as the period in which the sensor resistance reached 90% of the response value upon exposure to the explosive vapor, while the recovery time was defined as the period in which the sensor resistance changed to 10% of the response value after the explosive vapor was removed.

*Computational Details*: The initial nitro-explosives molecules of TNT, DNT, and PNT were first optimized using the generalized-gradient approximation (GGA) with the PW91 function,[44] and the double numerical basis set including d-polarization functions as implemented in the $DMOL^3$ package.[45,46] The resulting 3D periodic SiNW (with the length of 10 nm) and $TiO_2$ nanoparticles decorated SiNW systems were equilibrated using molecular dynamic simulation with DREIDING force field as implemented in the FORCITE package.[47] Here, the adsorption energy of the SiNW and the $TiO_2$ nanoparticles decorated SiNW toward TNT, DNT or PNT molecules were calculated according to the following equation. Take TNT as an example, $E_{ad} = E_{(TNT–TiO2/SiNW)} - E_{(TiO2/SiNW)} - E_{(TNT)}$, where $E_{ad}$ is the adsorption energy; $E_{(TNT–TiO2/SiNW)}$, $E_{(TiO2/SiNW)}$, and $E_{(TNT)}$ stand for the total energy of the $TiO_2$ nanoparticles decorated SiNW with the adsorption of TNT, the $TiO_2$ nanoparticles decorated SiNW, TNT systems, respectively.

## Supporting Information

Supporting Information is available from the Wiley Online Library or from the author.

## Acknowledgements

The authors thank the financial supports from the Xinjiang International Science and Technology Cooperation Program (20136008), Research Program of Chinese Academy of Sciences (CAS, CXJJ-14-M27), National Basic Research Program of China (2014CB931700/2014CB931702), the Xinjiang Program of Cultivation of Young Innovative Technical Talents (2013711015), National Natural Science Foundation of China (51372273, 61222403), Xinjiang Program of Introducing High Level Talents, Urumqi Talents Project (P141010001), "Hundred Talents Program" of CAS and SRF for ROCS, SEM. The authors also acknowledge Computer Network Information Center (Supercomputing Center) of CAS for allocation of computing resource.

Received: March 20, 2015
Revised: April 23, 2015
Published online: May 15, 2015

[1] P.-C. Chen, S. Sukcharoenchoke, K. Ryu, L. Gomez de Arco, A. Badmaev, C. Wang, C. Zhou, *Adv. Mater.* **2010**, *22*, 1900.
[2] R.-M. Ma, S. Ota, Y. Li, S. Yang, X. Zhang, *Nat. Nanotechnol.* **2014**, *9*, 600.
[3] J. M. Schnorr, D. van der Zwaag, J. J. Walish, Y. Weizmann, T. M. Swager, *Adv. Funct. Mater.* **2013**, *23*, 5285.
[4] S. Tamane, C. Topal, A. K. Kalkan, *IEEE-Nano* **2011**, *11*, 301.
[5] L. Guo, B. Zu, Z. Yang, H. Cao, X. Zheng, X. Dou, *Nanoscale* **2014**, *6*, 1467.
[6] Z. Yang, L. Guo, B. Zu, Y. Guo, T. Xu, X. Dou, *Adv. Opt. Mater.* **2014**, *2*, 738.
[7] B. Zu, Y. Guo, X. Dou, *Nanoscale* **2013**, *5*, 10693.
[8] D. Wang, H. Sun, A. Chen, S.-H. Jang, A. K.-Y. Jen, A. Szep, *Nanoscale* **2012**, *4*, 2628.
[9] Y. Engel, R. Elnathan, A. Pevzner, G. Davidi, E. Flaxer, F. Patolsky, *Angew. Chem. Int. Ed.* **2010**, *49*, 6830.
[10] D. Wang, A. Chen, S.-H. Jang, H.-L. Yip, A. K.-Y. Jen, *J. Mater. Chem.* **2011**, *21*, 7269.
[11] D. Wang, A. Chen, A. K.-Y. Jen, *Phys. Chem. Chem. Phys.* **2013**, *15*, 5017.
[12] G. S. Aluri, A. Motayed, A. V. Davydov, V. P. Oleshko, K. A. Bertness, M. V. Rao, *IEEE Sens. J.* **2013**, *13*, 1883.
[13] T.-Y. Wei, P.-H. Yeh, S.-Y. Lu, Z. L. Wang, *J. Am. Chem. Soc.* **2009**, *131*, 17690.
[14] P. H. Yeh, Z. Li, Z. L. Wang, *Adv. Mater.* **2009**, *21*, 4975.
[15] A. Singh, M. Uddin, T. Sudarshan, G. Koley, *Small* **2014**, *10*, 1555.
[16] F. Schedin, A. Geim, S. Morozov, E. Hill, P. Blake, M. Katsnelson, K. Novoselov, *Nat. Mater.* **2007**, *6*, 652.
[17] X. Li, X. Wang, L. Zhang, S. Lee, H. Dai, *Science* **2008**, *319*, 1229.
[18] X. Wang, L. Zhi, K. Müllen, *Nano Lett.* **2008**, *8*, 323.
[19] P. Blake, P. D. Brimicombe, R. R. Nair, T. J. Booth, D. Jiang, F. Schedin, L. A. Ponomarenko, S. V. Morozov, H. F. Gleeson, E. W. Hill, *Nano Lett.* **2008**, *8*, 1704.
[20] Y. Cao, J. Zhu, J. Xu, J. He, J. L. Sun, Y. Wang, Z. Zhao, *Small* **2014**, *10*, 2345.
[21] A. Fattah, S. Khatami, C. C. Mayorga-Martinez, M. Medina-Sánchez, L. Baptista-Pires, A. Merkoçi, *Small* **2014**, *10*, 4193.
[22] H. Yang, J. Heo, S. Park, H. J. Song, D. H. Seo, K.-E. Byun, P. Kim, I. Yoo, H.-J. Chung, K. Kim, *Science* **2012**, *336*, 1140.
[23] H. Han, J. Kim, H. S. Shin, J. Y. Song, W. Lee, *Adv. Mater.* **2012**, *24*, 2284.
[24] C. R. Field, H. J. In, N. J. Begue, P. E. Pehrsson, *Anal. Chem.* **2011**, *83*, 4724.
[25] X. Li, H. Zhu, K. Wang, A. Cao, J. Wei, C. Li, Y. Jia, Z. Li, X. Li, D. Wu, *Adv. Mater.* **2010**, *22*, 2743.

[26] L. Pinnaduwage, A. Gehl, D. Hedden, G. Muralidharan, T. Thundat, R. Lareau, T. Sulchek, L. Manning, B. Rogers, M. Jones, *Nature* **2003**, *425*, 474.
[27] N. Hannink, S. J. Rosser, C. E. French, A. Basran, J. A. Murray, S. Nicklin, N. C. Bruce, *Nat. Biotechnol.* **2001**, *19*, 1168.
[28] R. G. Ewing, M. J. Waltman, D. A. Atkinson, J. W. Grate, P. J. Hotchkiss, *Trends Anal. Chem.* **2013**, *42*, 35.
[29] C. Y. Chen, C. S. Wu, C. J. Chou, T. J. Yen, *Adv. Mater.* **2008**, *20*, 3811.
[30] Z. Huang, H. Fang, J. Zhu, *Adv. Mater.* **2007**, *19*, 744.
[31] B. Zu, B. Lu, Z. Yang, Y. Guo, X. Dou, T. Xu, *J. Phys. Chem. C.* **2014**, *118*, 14703.
[32] X. Dou, D. Sabba, N. Mathews, L. H. Wong, Y. M. Lam, S. Mhaisalkar, *Chem. Mater.* **2011**, *23*, 3938.
[33] J. Kim, S. D. Oh, J. H. Kim, D. H. Shin, S. Kim, S.-H. Choi, *Sci. Rep.* **2014**, *4*, 5384.
[34] C.-C. Chen, M. Aykol, C.-C. Chang, A. Levi, S. B. Cronin, *Nano Lett.* **2011**, *11*, 1863.
[35] S. M. Sze, *Physics of Semiconductor Devices*, Wiley, New York **1981**, pp. 245–297.
[36] X. Kong, C. Liu, W. Dong, X. Zhang, C. Tao, L. Shen, J. Zhou, Y. Fei, S. Ruan, *Appl. Phys. Lett.* **2009**, *94*, 123502.
[37] C. Crowell, S. Sze, *Solid-State Electron.* **1966**, *9*, 1035.
[38] Y. Che, X. Yang, G. Liu, C. Yu, H. Ji, J. Zuo, J. Zhao, L. Zang, *J. Am. Chem. Soc.* **2010**, *132*, 5743.
[39] Y. Liu, C.-L. Chen, Y. Zhang, S. R. Sonkusale, M. L. Wang, M. R. Dokmeci, *IEEE Sens. J.* **2013**, *13*, 202.
[40] G. He, N. Yan, J. Yang, H. Wang, L. Ding, S. Yin, Y. Fang, *Macromolecules* **2011**, *44*, 4759.
[41] W. S. Hummers, R. E. Offeman, *J. Am. Chem. Soc.* **1958**, *80*, 1339.
[42] Y. Xu, L. Zhao, H. Bai, W. Hong, C. Li, G. Shi, *J. Am. Chem. Soc.* **2009**, *131*, 13490.
[43] H. A. Becerril, J. Mao, Z. Liu, R. M. Stoltenberg, Z. Bao, Y. Chen, *ACS Nano* **2008**, *2*, 463.
[44] J. P. Perdew, Y. Wang, *Phys. Rev. B: Condens. Matter* **1992**, *45*, 13244.
[45] C. Sosa, J. Andzelm, B. C. Elkin, E. Wimmer, K. D. Dobbs, D. A. Dixon, *J. Phys. Chem.* **1992**, *96*, 6630.
[46] B. Delley, *J. Chem. Phys.* **2000**, *113*, 7756.
[47] S. L. Mayo, B. D. Olafson, W. A. Goddard, *J. Phys. Chem.* **1990**, *94*, 8897.